THE JOURNAL OF BIOLOGICAL CHEMISTRY VOL. 288, NO. 22, pp. 15590–15599, May 31, 2013

Diabetes-induced Central Neuritic Dystrophy and Cognitive Deficits Are Associated with the Formation of Oligomeric Reticulon-3 via Oxidative Stress*

Received for publication, December 3, 2012, and in revised form, April 14, 2013 Published, JBC Papers in Press, April 16, 2013, DOI 10.1074/jbc.M112.440784

Bei Zhao[‡§], **Bai-Shen Pan**[¶], **Su-Wen Shen**[‡§], **Xiao Sun**[‡§], **Zheng-Zhou Hou**[‡§], **Riqiang Yan**[‖], **and Feng-Yan Sun**[‡§1]

From the [‡]*Institutes for Biomedical Science and Department of Neurobiology of the School of Basic Medical Sciences, Shanghai 200032,* [¶]*Laboratory of Clinical Biochemistry, Zhongshan Hospital, Shanghai Medical College of Fudan University, Shanghai 200032, China , the* [‖]*Department of Neuroscience, Lerner Research Institute, The Cleveland Clinic Foundation, Cleveland, Ohio 44195 and the* [§]*State Key Laboratory of Medical Neurobiology, Shanghai Medical College of Fudan University, Shanghai 200032, China*

Background: Diabetes induces cognitive deficits and cortical lesion.
Results: Diabetes with cognitive deficits caused formation of carbonylated reticulon3 aggregates and reticulon3-immunoreactive dystrophic neurites.
Conclusion: Diabetes-induced central neuritic dystrophy was correlated with formation of oligomeric reticulon3 via oxidation.
Significance: Present findings concerning oxidative reticulon3 oligomers in formation of neuritic dystrophy may lead to explore a new therapeutic strategy for preventing/reducing diabetic dementia.

Diabetes is a high risk factor to dementia. To investigate the molecular mechanism of diabetic dementia, we induced type 2 diabetes in rats and examined potential changes in their cognitive functions and the neural morphology of the brains. We found that the diabetic rats with an impairment of spatial learning and memory showed the occurrence of RTN3-immunoreactive dystrophic neurites in the cortex. Biochemical examinations revealed the increase of a high molecular weight form of RTN3 (HW-RTN3) in diabetic brains. The corresponding decrease of monomeric RTN3 was correlated with the reduction of its inhibitory effects on the activity of β-secretase (BACE1), a key enzyme for generation of β-amyloid peptides. The results from immunoprecipitation combined with protein carbonyl detection showed that carbonylated RTN3 was significantly higher in cortical tissues of diabetic rats compared with control rats, indicating that diabetes-induced oxidative stress led to RTN3 oxidative damage. In neuroblastoma SH-SY5Y cells, high glucose and/or H_2O_2 treatment significantly increased the amounts of carbonylated proteins and HW-RTN3, whereas monomeric RTN3 was reduced. Hence, we conclude that diabetes-induced cognitive deficits and central neuritic dystrophy are correlated with the formation of aggregated RTN3 via oxidative stress. We provided the first evidence that oxidative damage caused the formation of toxic RTN3 aggregates, which participated in the pathogenesis of central neuritic dystrophy in diabetic brain. Present findings may offer a new therapeutic strategy to prevent or reduce diabetic dementia.

Alzheimer disease (AD)[2] is the most common cause of dementia, accounting for 60–80% of cases. Growing evidence indicates that AD often occurs along with other dementias (1). The pathological hallmarks of AD are the presence of substantial numbers of neurofibrillary tangles due to accumulation of abnormally hyperphosphorylated Tau (2) and senile plaques, which are composed of β-amyloid (Aβ) aggregates (3, 4). Aβ oligomers together with hyperphosphorylated Tau induce neuronal toxicity and axonal degeneration, which cause neuronal death via complex mechanisms (5, 6). Drugs currently available for treating dementia and AD have only minimal effects and do not impede disease progression significantly (7). Clinically, the symptoms of dementia gradually develop over many years or even decades. Therefore, the prevention of AD development is an alternative strategy for reducing the incidence of the disease. To delay the onset of symptoms, potentially modifiable risk factors for AD and dementia must be identified. A National Institutes of Health review reported that diabetes is one of the high risk factors for dementia and AD (8).

The incidence of diabetes mellitus (DM) continues to increase worldwide (9), and 90–95% of the diabetic cases are non-insulin-dependent diabetes mellitus (type 2 diabetes). Epidemiological studies clearly demonstrate an association between diabetes and dementia (10, 11). For example, diabetes or impaired fasting glucose is present in ~80% of AD patients (12); memory loss or cognitive decline in diabetic patients may be caused by vascular permeability and protein metabolism dysfunctions (13). Using different animal models, several groups have demonstrated that the activity of β-secretase

* This work was supported, in whole or in part, by National Institutes of Health Grant AG025493 (to R. Y.). This work was supported in part by grants from National Nature Science Foundation of China Grants 81030020, J0730860, and 30770660 (to F.-Y. S.).

[1] To whom correspondence should be addressed: Dept. of Neurobiology, Shanghai Medical College of Fudan University, 138, Yi-Xue-Yuan Rd., Shanghai 200032, China. Tel.: 86-21-54237652; Fax: 86-21-54237652; E-mail: fysun@shmu.edu.cn.

[2] The abbreviations used are: AD, Alzheimer disease; Aβ, β-amyloid; DM, diabetes mellitus; BACE1, β-secretase; RTN, reticulon; DNPH, 2,4-dinitrophenylhydrazine; DNP, dinitrophenyl; mono-RTN3 and RTN3, monomeric RTN3; RIDN, RTN3 immunoreactive dystrophy neurite; HW-RTN3, high molecular mass RTN3.

(BACE1) and the Aβ content are increased in DM genetic mouse brains (14) and type 2 diabetes rats (15). In addition, hyperphosphorylated Tau is increased in type 2 diabetes rat brains and negatively correlates with the changes in phosphorylated synaptophysin, a synaptic protein (16). Although other studies have suggested that increased Aβ generation in post-stroke brains is likely associated with increased stability of BACE1 via activation of caspase-3 (17, 18) and/or dysfunction of ubiquitin-mediated protein degradation (19), the molecular mechanisms underlying AD-like pathogenesis in diabetic brains remain unknown.

Reticulons (RTNs), a family of membrane-bound proteins consisting of four members (20), are widely distributed throughout the brain and play important roles in endocytosis (21), exocytosis (22), cellular trafficking, and neurite outgrowth (23). Elevated expression of RTNs in mouse and human brains appears to cause dysfunction in axonal generation and synaptic transmission (24, 25). Recent studies demonstrate that all four RTNs negatively modulate BACE1 activity (26, 27). RTN3, which is mainly expressed by neurons in the brain and co-localizes with BACE1 in neurons, is a potent BACE1 inhibitor (28). Functional studies indicate that a normal increase in RTN expression substantially reduces Aβ and overexpression of RTN3 in transgenic mouse brain induces the formation of RTN3 aggregates in neurites, causing neuritic dystrophy and impairment of spatial learning and memory as well as synaptic plasticity (29). Further studies demonstrate that preformed RTN3 aggregates reduce dendritic spine density and synaptic function in transgenic mouse brains (30). Therefore, RTNs are emerging as critical factors in the pathogenesis of neurodegenerative diseases.

It has been well demonstrated that the advanced stages of diabetes usually result in sensory and autonomic neuropathy in the peripheral nervous system and white matter lesions as well as cortical and subcortical atrophy in the central nervous system, which has been indicated by magnetic resonance image (31). Because RTN3-mediated neuritic dystrophy is linked to Alzheimer cognitive dysfunction, we therefore asked whether RTN3-mediated neuritic dystrophy occurred in the frontal parietal cortex of diabetic rats and whether its occurrence would contribute to diabetic dementia. To address these questions, we used an induced type 2 diabetes rat model to observe changes in cognitive function and neuronal morphology in diabetic brains. The results demonstrated that monomeric RTN3 and its interaction with BACE1 were decreased in diabetic rats and that these changes were followed by an increase in Aβ formation in the cortex. Furthermore, RTN3 aggregates densely accumulated in neurites immunopositive for RTN3 oligomers but not the neuritic marker SMI32. Further studies indicated that oxidative stress might cause the formation of RTN3 oligomers and promote neuritic dystrophy in diabetic brains. Behavioral tests further revealed cognitive deficits in diabetic rats. Collectively, these results reveal a novel molecular mechanism of diabetic dementia and suggest a new therapeutic strategy for preventing or reducing the development of dementia in type 2 diabetes patients.

EXPERIMENTAL PROCEDURES

Diabetic Rat Model and Tissue Preparation—Adult male Sprague-Dawley rats (200–220 g) from the Shanghai Experimental Animal Center (Chinese Academy of Sciences, China) were used. Animal experiments were carried out in accordance with the National Institutes of Health guide for the care and use of laboratory animals.

Rats were divided into control and diabetic (DM) groups and fed with commercially available normal pellet diet (NPD) (10% calories as fat) or in-house prepared high fat diet (60% calories as fat, and the diet composition included 425 g·kg^{-1} powdered NPD, 310 g·kg^{-1} lard, 250 g·kg^{-1} casein, 10 g·kg^{-1} cholesterol, DL-methionine, 1 g·kg^{-1} yeast powder, 1 g·kg^{-1} sodium chloride) for a period of 2 months based on previously published protocols (15, 16). The high fat diet rats were injected intraperitoneally with streptozotocin (25 mg·kg^{-1}, Alexis, Exeter, UK) and then fed with their original diet for another month. Plasma glucose, triglyceride, and cholesterol levels were measured with a Hitachi Model 7600 Series Automatic Analyzer (Hitachi High-Technologies Corp.). To analyze the insulin sensitivity of rats, a simple intravenous insulin glucose tolerant test was performed as previously described (32). Briefly, after rats were anesthetized by intraperitoneal injection 10% chloral hydrate (360 mg·kg^{-1}), two femoral blood vessels were exposed by incision through the skin in the inguinal area. These vessels were cannulated with plastic fine cannulae, and then the intravenous insulin glucose tolerant test was performed. The rats were subsequently injected with glucose (0.7 g·kg^{-1}) and insulin (0.175 units·kg^{-1}) into the femoral vein. Blood samples were then withdrawn from the femoral artery at ~0 (before glucose), 2, 4, 6, 8, 10, 20, and 30 min after insulin injection for the glucose estimation. The equivalent volume of sterile saline (0.9%) was injected into femoral vein after each sampling to prevent the changes in central compartmental blood volume. Insulin sensitivity was determined by the glucose disappearance rate within 10 min, evident from the average slope K in the curve fitted by log-linear regression over this period. Rats with blood glucose higher than 18 mmol/liter were defined as diabetic animals.

Morris Water Maze Test—Rats were subjected to the Morris water maze test to analyze cognitive function as previously reported (15, 33). The Morris water maze test consisted of a non-visible platform trial, a probe trial, and a visible platform trial. Rats received the non-visible platform trial twice per day (every morning and afternoon) for the first 5 days, a probe trial on the 6th day, and a visible platform trial on the 7th day. The swimming path and the escape latency (time to reach the platform) were recorded in real time by video camera assisted with Microcomputer Running Maze Software (Shanghai Jiliang Software Technology Co., Ltd.). The mean escape latency, the percentage of time spent in the right quadrant, and the velocity (mm/s) were calculated and used for statistical analysis.

Immunohistochemical Staining—Animals were deeply anesthetized and quickly subjected to transcardial perfusion with freshly prepared 0.9% saline solution followed by 4% paraformaldehyde in phosphate-buffer solution (0.1 M, pH 7.4, PBS). Then coronal sections at a thickness of 30 μm were cut on a freezing microtome (Jung Histocut, Model 820-II, Leica, Ger-

many) at the bregma level from −2.30 to −3.30 mm. Brain sections were probed with primary antibodies (rabbit polyclonal anti-BACE1 antibody B690, 1:1000 (Calbiochem) or mouse monoclonal anti-A$\beta_{x\text{-}42}$ antibody, 1:200 (Millipore) and corresponding biotinylated secondary antibodies (1:200, Vector Laboratories) followed by avidin-biotin-peroxidase (1:200, Vectastain Elite ABC kit, Vector Laboratories). Immunoreactivity was visualized with 0.05% diaminobenzidine (Sigma) as the chromogen. Negative controls received the same treatment, except that primary antibodies were omitted, and showed no specific staining.

Fluorescence Immunolabeling and Confocal Scanning—For double staining of RTN3 with NeuN, SMI32, or oligomers, free-floating sections were incubated with rabbit polyclonal anti-RTN3 antibody (R458, 1:1000) and then incubated with anti-rabbit IgG-FITC (1:40, Santa Cruz Biotechnology). After washing in PBS, sections were incubated with mouse monoclonal anti-NeuN antibody (1:1000, Abcam), mouse monoclonal anti-SMI32 antibody (1:1000, Abcam), mouse monoclonal anti-AT8 antibody (1:60, Innogenetics), or rabbit monoclonal antibody against oligomers (Invitrogen) and then incubated with anti-mouse IgG-rhodamine (NeuN, SMI32, AT-8) or anti-rabbit IgG-rhodamine (oligomer) (1:50, Roche Diagnostics). Fluorescent signals were detected using a confocal laser scanning microscope (TCS SP5, Leica).

Immunohistochemical Staining for 8-OxodG—The immunostaining were carried out based on a previous report (34). Briefly, the sections were incubated with 100 μg/ml RNase in 10 mM Tris buffer containing 1 mM EDTA, 400 mM NaCl (pH 7.5) for 60 min at 37 °C and with 2 N HCl for 10 min at room temperature and then neutralized with 50 mM Tris buffer for 5 min at room temperature. The sections were blocked with 10% fetal bovine serum in 10 mM Tris buffer (pH 7.5) for 60 min at 37 °C and incubated with mouse anti-8-oxodG monoclone antibody (1:1000, R&D system, Inc.) overnight at 4 °C. After washing, the sections were incubated with biotinylated anti-mouse IgM (1:200) for 60 min and with avidin-biotin-peroxidase (1:200, Vectastain Elite ABC kit). Immunoreactivity was visualized with 0.05% diaminobenzidine as the chromogen. Negative controls received the same treatment, except that primary antibodies were omitted and showed no specific staining.

RT-PCR—Total RNA was extracted using TRIzol reagent (Invitrogen) according to the manufacturer's instructions. Total RNA (5 μg) from cortex was used for RT-PCR. The primers were as follows: β-actin (accession number NM031144), forward (gtcttcccctccatcgtggg) and reverse (tggctggggtgttgaaggtc), resulting in a 306-bp product; RTN3 (accession number NM 080909.2), forward (ctggcagctttcagtgtt) and reverse (aatgggaagactaagagcg), resulting in a 204-bp product. Reactions were performed in a final volume of 25 μl with Taq polymerase (5 units/μl, Tiangen Biotech, Beijing, China) for 30 cycles. Each PCR product (20 μl) was electrophoresed on a 2% agarose gel containing 0.5 μg/ml ethidium bromide, visualized using an ultraviolet transilluminator (Image Master VDS, Bio-Rad) and photographed.

Aβ_{40} and Aβ_{42} Measurement—Aβ_{40} and Aβ_{42} were detected by enzyme-linked immunosorbent assay (ELISA) using the high sensitivity Aβ_{40} (KHB3481)- and Aβ_{42} (KHB3441)-specific ELISA kits (Invitrogen). Briefly, the samples of rat wet brain were weighed and dissolved in cold 50 mM Tris/5 M guanidine buffer (pH 8.0) to achieve the final concentration, 1 mg/μl. Then tissues were ground thoroughly, and homogenates were mixed at room temperature for 4 h. Homogenates were diluted 1:20 with cold reaction buffer containing 0.2 g·liter^{-1} KCl, 0.2 g·liter^{-1} KH_2PO_4, 8.0 g·liter^{-1} NaCl, 1.15 g·liter^{-1} Na_2HPO_4, 5% BSA, 0.03% Tween 20, and 1× protease inhibitor mixture (Complete Protease Inhibitor Mixture tablet, Roche Diagnostics) then centrifuged at 16,000 × *g* for 20 min at 4 °C. Supernatants were collected, and protein concentrations were determined by a BCA kit (Beyotime, Shanghai, China). Then Aβ_{40} and Aβ_{42} levels were determined by comparison with the respective standard curves following the manufacturer's protocol.

Western Blot Analysis—Equal amounts of protein from cerebral cortex tissue extracts or cell lysates were electrophoresed on 12% sodium dodecyl sulfate-PAGE gels and then transferred to polyvinyl difluoride membranes. Anti-RTN3 antibody (1:2000), anti-BACE1 antibody (1:1000), and anti-APP-C-terminal antibody (1:2000, Sigma) were used to detect the levels of these specific proteins. Horseradish peroxidase-conjugated goat anti-rabbit/mouse IgGs (1:3000, Santa Cruz Biotechnology) were used as secondary antibodies, and Western blotting luminescent reagent was used to visualize peroxidase activity. Normalization was carried out by stripping the blots and reprobing with a mouse monoclonal antibody to the β-isoform of actin (1:10,000, Sigma). Optical densities of immunostained bands were analyzed with an image processing and analysis system (Image J 1.37 software, National Institutes of Health).

Immunoprecipitation and Western Blot Analysis—Tissue extracts (200 μg of protein) were first incubated with 1 μl of anti-BACE1 antibody, rabbit polyclonal anti-oligomer antibody (BIOSOURCE International, Inc.) or anti-RTN3 antibody in 50 mM Tris buffer containing 1 mM EDTA, 10% glycerol, 1 μM Na_3VO_4, 10 mM NaF, and a protease inhibitor mixture for 12 h at 4 °C and then with protein-A beads for 2 h. The reactions were centrifuged at 10,000 rpm to obtain the immunoprecipitates, which were analyzed by Western blotting with anti-RTN3 (1:2000) or anti-BACE1 (1:1000) antibodies as described above.

Cell Culture and Treatment—The human neuroblastoma SH-SY5Y cell line was cultured in 6-well plates with Dulbecco's modified Eagle's medium (Invitrogen) supplemented with 15% (v/v) fetal bovine serum (Invitrogen) at 37 °C in a humidified 5% CO_2 atmosphere. Once cells reached 80–90% confluence, the cultures were incubated in medium containing 300 μM H_2O_2, 500 μM H_2O_2, 25 mM glucose, 300 μM H_2O_2 + 25 mM glucose, or 500 μM H_2O_2 + 25 mM glucose for 1 h, then harvested for RTN3 and protein carbonyl detection. Cells were cultured with medium containing 0.5% DMSO (vehicle) as a control.

Protein Carbonyl Detection—Protein carbonyl adduct formation was used to identify oxidized proteins as previously described (35). Briefly, cortical lysates (20 μg of protein) or cell lysates (40 μg of protein) were first reacted with 10 mmol of 2,4-dinitrophenylhydrazine (DNPH) in 2 N HCl for 20 min to enable adduct formation by the dinitrophenyl (DNP) group and then the reaction was quenched by using 1 M Tris solution. The samples containing protein carbonyls/DNP-modified proteins

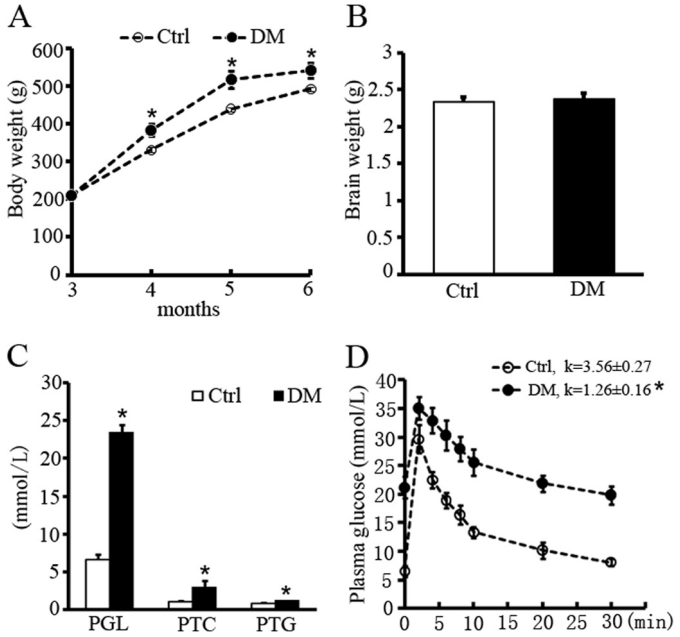

FIGURE 1. **Changes of body weight, biochemical parameters, and insulin sensitivity in diabetic rats.** Body weight, plasma glucose (*PGL*), plasma total cholesterol (*PTC*), and plasma triglyceride (*PTG*), brain weight, and insulin sensitivity were determined in diabetic rats. Compared with control (*Ctrl*, $n = 10$) rats, DM ($n = 15$) rats showed time-dependent increases in body weight within 3 months (*A*) and increased in glucose, cholesterol, and triglyceride (*C*) but showed no changes in brain weight (*B*). An intravenous insulin glucose tolerance test was performed to calculate the *k* value based on the glucose disappearance rate within 10 min by the average slope. These results demonstrated that the *k* value decreased in DM rats (*D*, $n = 5$/group), indicating reduced insulin sensitivity in the diabetic rats. Data are shown as the mean ± S.E. * represents $p < 0.05$ *versus* the controls.

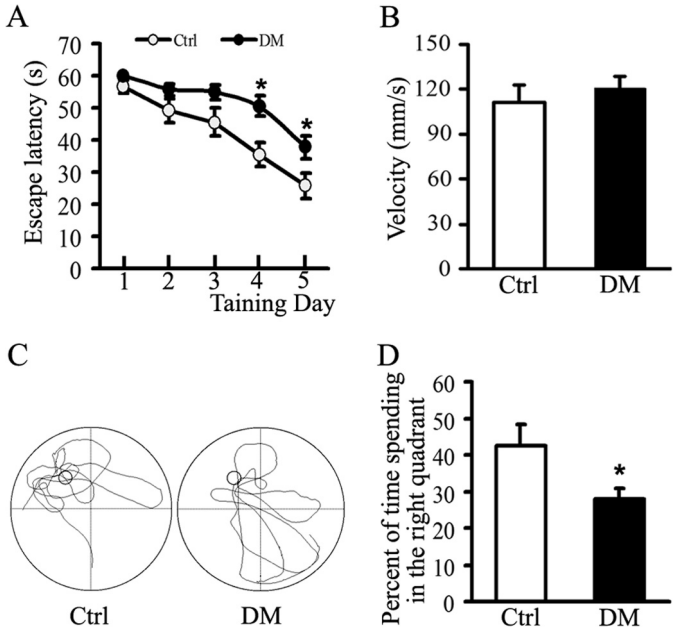

FIGURE 2. **Diabetic rats showed impaired performance in water maze tests.** *A*, in non-visible trials, diabetic rats took longer to find the platform on training days 4 and 5 compared with control (*Ctrl*) rats. *B*, in visible platform trials, rats showed similar motor function in the control and diabetic groups. *C* and *D*, in probe trials, typical swimming patterns were recorded on training day 6 in both the control and diabetic rats (*C*), and the results showed that diabetic rats spent significantly less time in the target quadrant (*D*). All values are reported as the means ± S.E. ($n = 8$ and 9 for control and diabetic group, respectively). * represents $p < 0.05$ compared with the controls.

were analyzed by Western blotting with goat anti-DNP antibody (1:2000, Abcam). For analyzing carbonylated RTN3, total proteins from the carbonylated samples were immunoprecipitated with anti-DNP, purified with protein-A beads, and analyzed by Western blotting with anti-RTN3 antibody.

Data Quantification and Statistical Analysis—Optical densities of immunoblot and PCR bands were determined using Image J software. Densitometric quantification of HW-RTN3/RTN3 and RTN3mRNA was normalized to β-actin. All cells with positive staining in immunochemistry detection were counted in the fields of view and were repeated in four sections for each group. The significance of difference between control and DM groups was analyzed by unpaired two-tailed Student's *t*-tests, and multiple groups statistical differences in SH-SY5Y experiment were determined using one-way analysis of variance followed by Least Significant Difference tests. All values are presented as the means ± S.E. $p < 0.05$ was considered statistically significant.

RESULTS

Impairment of Cognitive Behavior in Diabetic Rats—To verify the establishment of the diabetic model, we measured body weight, total levels of cholesterol, triglyceride, and glucose in the blood plasma and detected insulin sensitivity by glucose tolerant test. Our results indicated that the rats in the DM group exhibited a significant increase in body weight as well as significantly higher levels of cholesterol, triglyceride, and glucose compared with the control group, whereas brain weight did not change (Fig. 1, *A*–*C*). Furthermore, glucose disappearance rates (*k* value) were significantly reduced in the diabetic rats compared with that in the controls (Fig. 1*D*), confirming that the diabetic rats were insulin-resistant.

To test whether the above changes would affect cognitive function in rats, we performed Morris water maze tests. We observed that diabetic rats took a longer time to find the platform on training days 4 and 5 compared with the control rats in the non-visible trials (Fig. 2*A*). In the probe trials, diabetic rats spent less time in the target quadrant compared with control rats (Fig. 2*C*), and these differences were statistically significant (Fig. 2*D*). Furthermore, no difference in swim speed was observed in the visible trials (Fig. 2*B*). These results indicate the impairment of spatial learning and memory in the diabetic rats.

Characteristics of RTN3 Protein Expression in Diabetic Brains—To determine the molecular linkage underlying the impairment of cognitive function in diabetic rats, we set out to examine the changes in RTN3, a protein known to negatively modulate BACE1 activity. RT-PCR and Western blotting were used to determine the changes in RTN3 mRNA and protein expression in rat brains. Consistent with previous reports (29, 36), we detected several forms of RTN3 in rat brains within molecular masses of ~24 kDa (monomeric RTN3 (mono-RTN3 or *RTN3*)) and 175 kDa (high molecular mass RTN3 (*HW-RTN3*)) (Fig. 3*A*). Interestingly, we found that mono-RTN3 was significantly reduced in DM rats compared with the controls (Fig. 3*B*). In contrast, HW-RTN3 levels were increased in the cortex of DM brains compared with controls. However, there was no obvious difference in the expression of RTN3 mRNA between DM and control rats (Fig. 3, *C* and *D*).

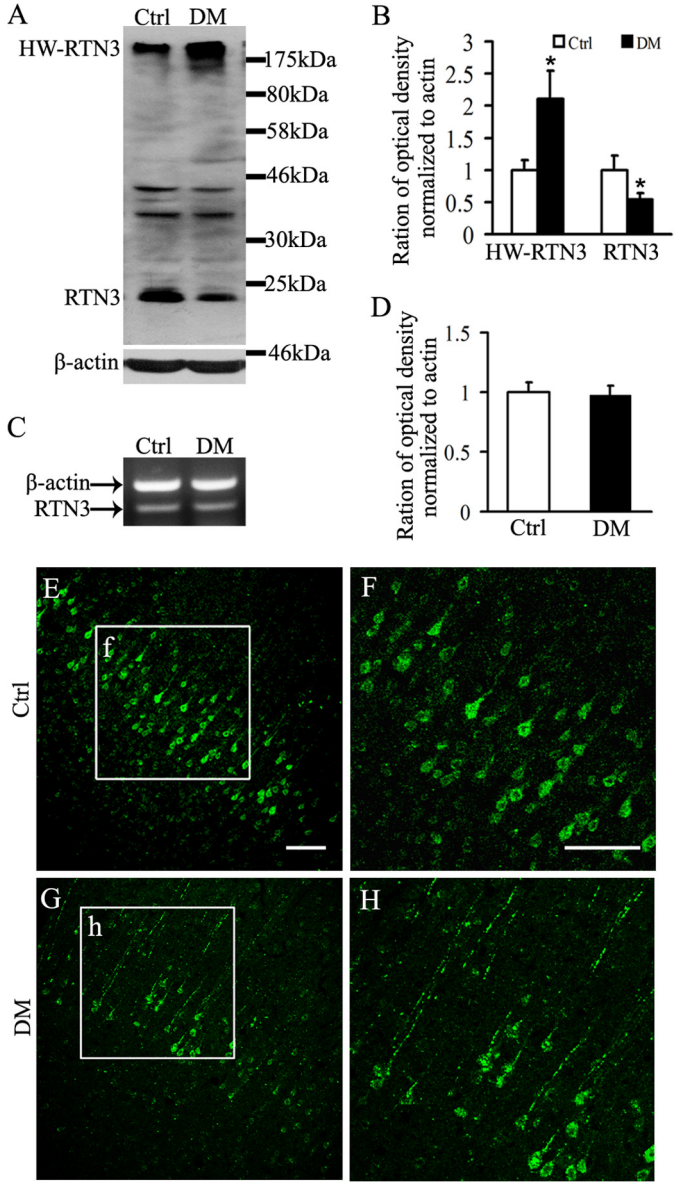

FIGURE 3. **Diabetes induced changes in RTN3 protein expression in rat brains.** *A*, tissue extracts from cortex in control and diabetic brains were analyzed by Western blotting with antibody R458 to the RTN3 C terminus. Bands near 24 kDa and above 175 kDa, respectively, demonstrated the presence of RTN3 and HW-RTN3 proteins ($n = 4$ in each group). *B*, HW-RTN3 proteins were increased, whereas monomeric RTN3 proteins were reduced in the cortex of diabetic rats compared with controls. *C* and *D*, RTN3 mRNA was detected by RT-PCR analysis (*C*) and showed no significant changes in the cortex (*D*) between control and diabetic brains ($n = 3$ in each group). Data are represented as the mean ± S.E. * represents $p < 0.05$ compared with the controls. *E–H*, shown is immunofluorescence staining of RTN3 in the parietal cerebral cortex of control (*E* and *F*) and diabetic rats (*G* and *H*). Photographs *F* and *H* are magnified images corresponding to the squares labeled with *f* and *h* in photos *E* and *F*, respectively.

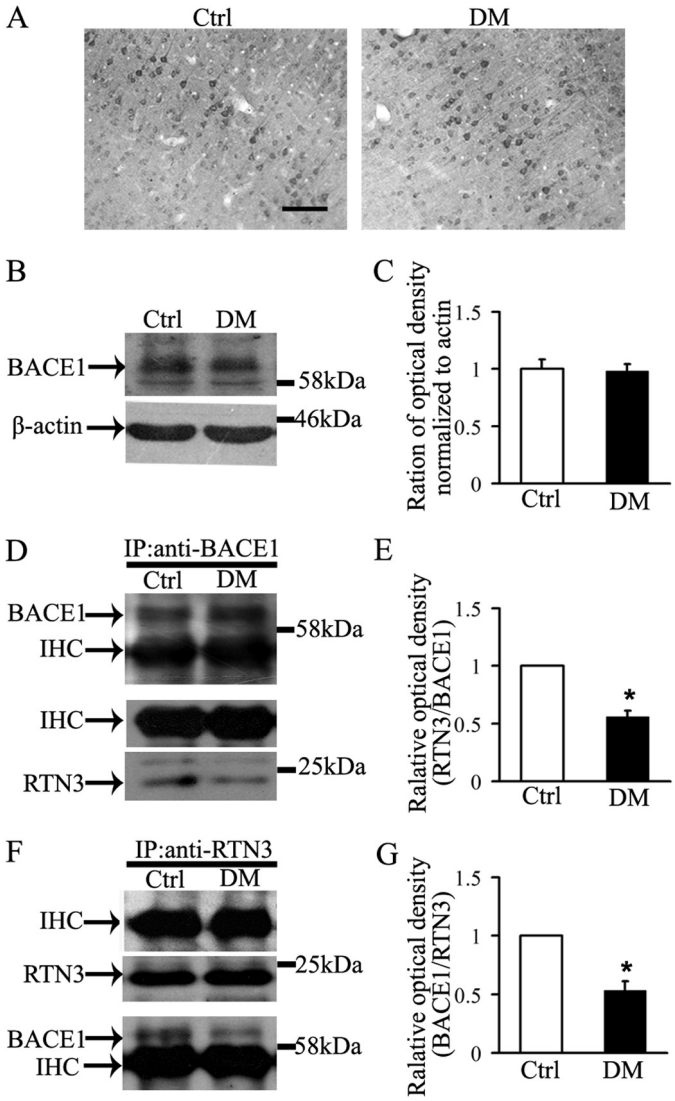

FIGURE 4. **Diabetic rats showed reduced interaction of RTN3 with BACE1 in rat brain.** *A*, BACE1-immunostained cells were present in the pyramidal neurons of the parietal cerebral cortex in control (*Ctrl*) and diabetic (*DM*) rats. *Bar* = 100 μm. *B* and *C*, tissue lysates extracted from cortex were used to examine BACE1 levels by Western blotting. The results show that the levels of BACE1 expression in the cortex were not significantly different between control and diabetic rats. *D* and *E*, enriched total tissue extract from control and diabetic rat brains (200 μg) were immunoprecipitated (*IP*) with a limited amount of anti-BACE1 antibody (1 μl) and then examined by Western blotting with anti-RTN3 (R458) antibody. The results show that BACE1-RTN3-binding proteins, but not BACE1 protein, were reduced in diabetic cortex. *F* and *G*, in the reversed immunoprecipitation assay, tissue lysates (200 μg) were immunoprecipitated with R458 antibody (1 μl) and examined by BACE1 antibody. The results show that BACE1-RTN3 binding proteins, but not RTN3 protein, were reduced in the diabetic cortex. *IHC* in *D* and *F*, IgG heavy Chain. Data are shown graphically as the mean ± S.E. ($n = 4$ per group). * represents $p <$ 0.05 compared with the controls.

Further immunostaining results showed that RTN3-positive (RTN3$^+$) staining was evenly distributed in the soma of pyramidal neurons in the cerebral cortex of the brains in the control rats (Fig. 3, *E* and *F*). Noticeably, in DM rats, RTN3$^+$ staining was not restrictively distributed in the soma of neurons. Rather, it also formed high density spots in the neurites of the prefrontal and parietal cortical regions (Fig. 3, *G* and *H*).

Reduced Mono-RTN3 Interactions with BACE1 and Increased BACE1 Activity in Diabetic Brains—It was previously reported that monomeric RTN3 inhibits the proteolytic activity of BACE1, a key enzyme for Aβ generation (28, 36). Therefore, we examined the interaction of RTN3 with BACE1 in DM rats. We found that BACE1+ neurons were similarly present in control and DM rat brains (Fig. 4*A*), and the levels of BACE1 protein appeared to be similar in both groups (Fig. 4, *B* and *C*). Coimmunoprecipitation using anti-BACE1 antibody showed

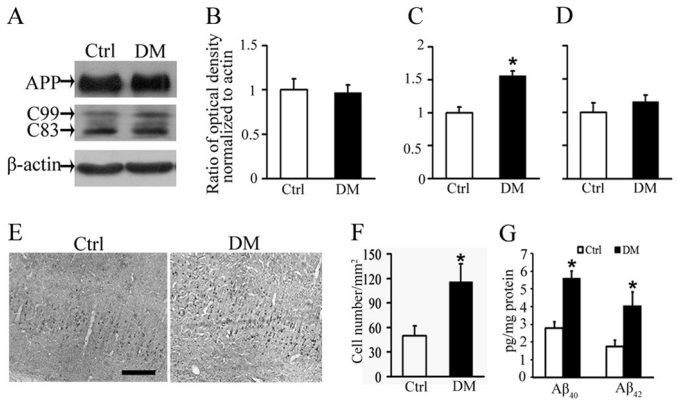

FIGURE 5. **Diabetes induced Aβ generation via increased BACE1 activity in rat brain.** *A*, Western blots revealed bands for full-length APP (FL-APP), APP-C99, BACE1-cleaved APP product, and APP-C83, an α-secretase cleaved product, in the cortex of control (*Ctrl*) and diabetic (*DM*) rats. Ratios of densitometry over actin were calculated and are represented graphically for FL-APP (*B*), APP-C99 (*C*), and APP-C83 (*D*) in the cortex. *E*, photos show Aβ immunopositive stained (Aβ^+) cells in the cortex of control and diabetic rat brains. *Bar* = 100 μm. Diabetes significantly increased the number of Aβ^+ cells in cortical neurons (*F*) and the amounts of $A\beta_{40}$ and $_{42}$ in cortical tissues (*G*). All values are reported as the means ± S.E. (n = 5 per group). * represents $p <$ 0.05 compared with the controls.

that RTN3 could directly bind to BACE1, but complexes of RTN3 with BACE1 were reduced in diabetic brains (Fig. 4, *D* and *E*). When we performed a reverse coimmunoprecipitation by pulling down protein complexes with anti-RTN3 antibody and used anti-BACE1 antibody for Western blotting, we further confirmed a reduced binding of BACE1 and RTN3 in diabetic rat brains (Fig. 4, *F* and *G*).

Based on published knowledge, RTN3 negatively regulates BACE1 enzyme activity through its binding to BACE1 (36). In this study we therefore asked if the activity of BACE1 was increased after the reduction of BACE1-RTN3 complexes in diabetic brains. It is well known that APP is cleaved by β-secretase and α-secretase to generate APP-C99 and APP-C83, and changes in these fragment levels are associated with either of these two enzymes. We found that APP-C99 was significantly increased in diabetic brains, whereas changes in APP levels were less obvious (Fig. 5, *A–D*), suggesting that BACE1 activity in diabetic brains was relatively increased compared with the controls.

We also performed immunostaining and ELISA to examine the number of Aβ^+-stained cells and the contents of Aβ in rat brains, respectively. Consistent with the elevated BACE1 activity, we indeed observed increased Aβ^+ stained cells in cortical neurons of diabetic brains (Fig. 5, *E* and *F*) as well as the levels of $A\beta_{40}$ and $A\beta_{42}$ in diabetic cortical tissues of rats (Fig. 5*G*).

Formation of RTN3 Aggregates and RTN3-associated Dystrophic Neurites in DM Brains—Results from double immunefluorescence further indicated that RTN3$^+$ and NeuN$^+$ double-labeled signals were evenly distributed in neural cell bodies in control rats, but RTN3$^+$ single-labeled signals formed higher density spots in the neurites in DM rat cortex (Fig. 3, *G* and *H*, and Fig. 6, *A* and *B*). In diabetic brains, positive staining of SMI32, a specific axonal marker protein, was reduced compared with controls. It should be noted that RTN3 did not co-stain with SMI32 (Fig. 6, *C* and *D*), suggesting that the neurites with RTN3$^+$ high density spots are devoid of normal axonal proteins and represent a dystrophic pathology.

Previous study suggested that RTN3$^+$ high density spots contain RTN3 aggregates (29). Results from our immunostaining and immunoprecipitation experiments showed that most RTN3$^+$ spots in neurites co-stained with an oligomer antibody (Fig. 6, *E* and *F*). Moreover, HW-RTN3 protein was precipitated with anti-oligomer antibody in the cortex of DM brains (Fig. 6*G*), indicating that DM induced an increase of RTN3 oligomers.

Accumulation of Oxidatively Damaged DNA and Protein in Diabetic Brains—To explore the mechanism underlying the formation of RTN3$^+$ spots in neurites, we hypothesized that oxidative stress might contribute to RTN3 oligomerization. By performing various biochemical assays, we detected an increase of 8-oxo-dG$^+$ immunoreactive cells in rat brains (Fig. 7*A*). The number of 8-oxo-dG$^+$ cells was 52.3 ± 9.6 cells/mm^2 in the control group and 105.8 ± 14.5 cells/mm^2 in the DM group, suggesting increased oxidative damage of DNA in diabetic brains. This observation prompted us to study whether proteins, particularly RTN3, were oxidatively damaged in diabetic brains. Free carbonyl side groups are considered to be an indicator of oxidatively damaged proteins. Protein carbonyls react with DNPH to form DNP, which can be detected with anti-DNP antibody. DNPH-reacted samples were analyzed by Western blotting with anti-DNP antibody, and we found that the numbers and densities of DNP-modified protein bands were increased in diabetic brains (Fig. 7, *B* and *C*). These data suggest that diabetes increases the amounts of oxidatively damaged proteins in the brain.

Next, we investigated if RTN3 proteins were oxidatively damaged in diabetic brains. An anti-DNP antibody was used to immunoprecipitate total carbonyl-containing proteins, and anti-RTN3 antibody was used to detect RTN3 carbonyls on Western blots. Interestingly, we found that monomeric RTN3 was precipitated with anti-DNP antibody in diabetic brains but not in control brains (Fig. 7, *D*, Ctrl+DNPH and DM+DNPH lanes, and *E*). Further studies indicated that aggregated RTN3 became monomeric after derivatization with DNPH in acidic conditions because treatment with or without hydrochloride solution enabled detection of mono-RTN3 only or both mono-RTN3 and HW-RTN3 bands, respectively (Fig. 7*D*, *third* and *fourth lanes*). This phenomenon indicated that RTN3 aggregates were not stable in this experimental condition, which may explain why RTN3 precipitated with anti-DNP antibody was mostly monomeric. This result also indicates that diabetes induces oxidative damage of RTN3 in the brain.

RTN3 Aggregation in SH-SY5Y Cells under Oxidative Stress—To confirm if oxidative stress or high glucose induced RTN3 aggregation in neurons, we further investigated the changes in RTN3 expression and protein carbonyls in cultured human neuroblastoma SH-SY5Y cells after treatment with different concentrations of H_2O_2 or/and glucose. Interestingly, we found that glucose (25 mM) and/or H_2O_2 (300 or 500 μM) could significantly increase the formation of oxidatively damaged proteins because the numbers and densities of DNP-modified protein bands were significantly increased compared with controls (Fig. 8, *A* and *B*). Under these experimental conditions, we also

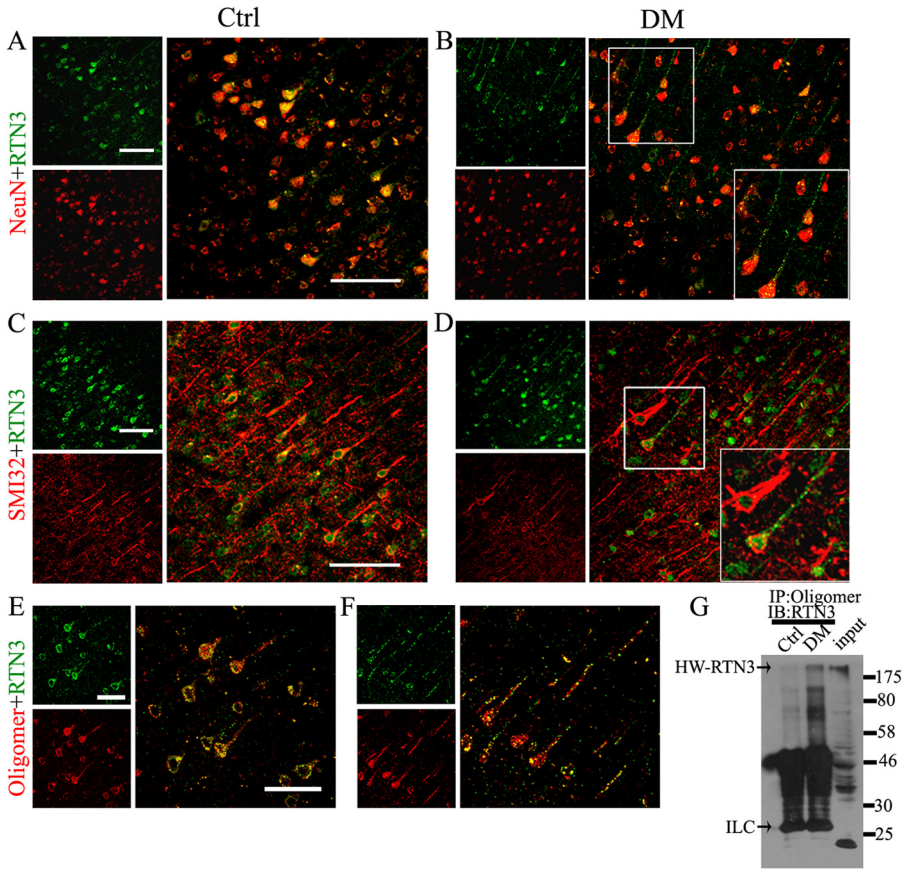

FIGURE 6. **Diabetes triggered the formation of RTN3 oligomer aggregates and neuritic dystrophy in rat brain.** Double fluorescent immunostaining of RTN3 with NeuN (*A* and *B*), SMI32 (*C* and *D*), or oligomer (*E* and *F*) in the parietal cerebral cortex of control (*A, C,* and *E*) and diabetic rats (*B, D,* and *F*). The *bar* = 100 μm in photos *A–D*, and the *bar* = 50 μm in photos (*E* and *F*). The images show that RTN3-positive ($RTN3^+$) staining was evenly distributed in neuronal cell bodies in control rats and co-localized with the neuronal marker, NeuN (*A*). $RTN3^+$ neurites in diabetic rats did not stain with NeuN (*B*) and SMI32 (*D*) but were co-stained by oligomer (*F*). *G*, tissue extracts (200 μg of protein) from the cortex were first precipitated (*IP*) with oligomer antibody (1 μl) and then detected on Western blots (*IB*) with RTN3 antibody. An *arrowhead* in *G* indicates IgG light chain (*ILC*). The results showed that HW-RTN3 was present in diabetic rat brains (*input*) and could be precipitated by anti-oligomer antibody in diabetic brains tissues (DM) but not in control tissues (*Ctrl*).

found that H_2O_2 and/or high glucose treatment increased HW-RTN3 and reduced mono-RTN3 (Fig. 8, *C* and *D*). These data were comparable with the results from the *in vivo* study as described above. Therefore, these results suggest that oxidative damage may induce RTN3 aggregation in diabetic brains.

DISCUSSION

In the present study we used a high fat diet combined with a single low dose injection of streptozotocin to induce type 2 diabetes with cognitive deficiency in rats, as demonstrated by blood tests (Fig. 1) and learning and memory-associated behavioral tests (Fig. 2). With this animal model, we revealed that diabetes reduced both the expression of monomeric RTN3 and the inhibitory effect of RTN3 on the activity of BACE1, thus leading to an increase in Aβ generation. Furthermore, diabetes induced RTN3 oxidative damage and oligomer formation, thereby inducing neuritic dystrophy in the brain. Taken together, diabetes-induced RTN3 changes may accelerate central neuritic dystrophy and further cause dysfunction of synaptic transmission and behavioral deficiency.

RTNs regulate neurite growth and synaptic plasticity in normal brain (37). Among them, RTN3 has been recognized as the most important RTN protein involved in the pathogenesis of neurodegenerative diseases. Interestingly, we found that RTN3 participates in the induction of neuronal pathology in diabetic rat brains because diabetes reduced the levels of monomeric RTN3 and increased the formation of oligomeric RTN3 (Figs. 3 and 6), which are associated with neurodegeneration and neurological dysfunction (29, 30). In fact, mono-RTN3 endogenously inhibits BACE1 enzyme activity via complex formation between RTN3 and BACE1 (30, 36). Therefore, mono-RTN3 reduction will theoretically cause an increase in BACE1 activity and Aβ generation. We found a decrease in the amounts of both RTN3 monomer and RTN3-BACE1 complexes (Fig. 4) and an increase in both the formation of APP-C99, a BACE1 cleavage product, and Aβ in diabetic brains (Fig. 5). Thus, these results suggest that diabetes stimulates BACE1 activity and Aβ generation in the brain at least partly via reduction of RTN3 monomer and its binding to BACE1.

Previous studies have demonstrated that RTN3 overproduction in the brain causes accumulation of RTN3-containing aggregates in dystrophic neurites, named as RTN3 immunoreactive dystrophy neurites (RIDNs) (29). In this present study we detected increased formation of RTN3 aggregates (HW-RTN3) in diabetic brains (Fig. 3). Moreover, HW-RTN3 could be precipitated by oligomer antibody and co-localized with oligomer in neurons (Fig. 6, *E–G*). Furthermore, we found neuritic dys-

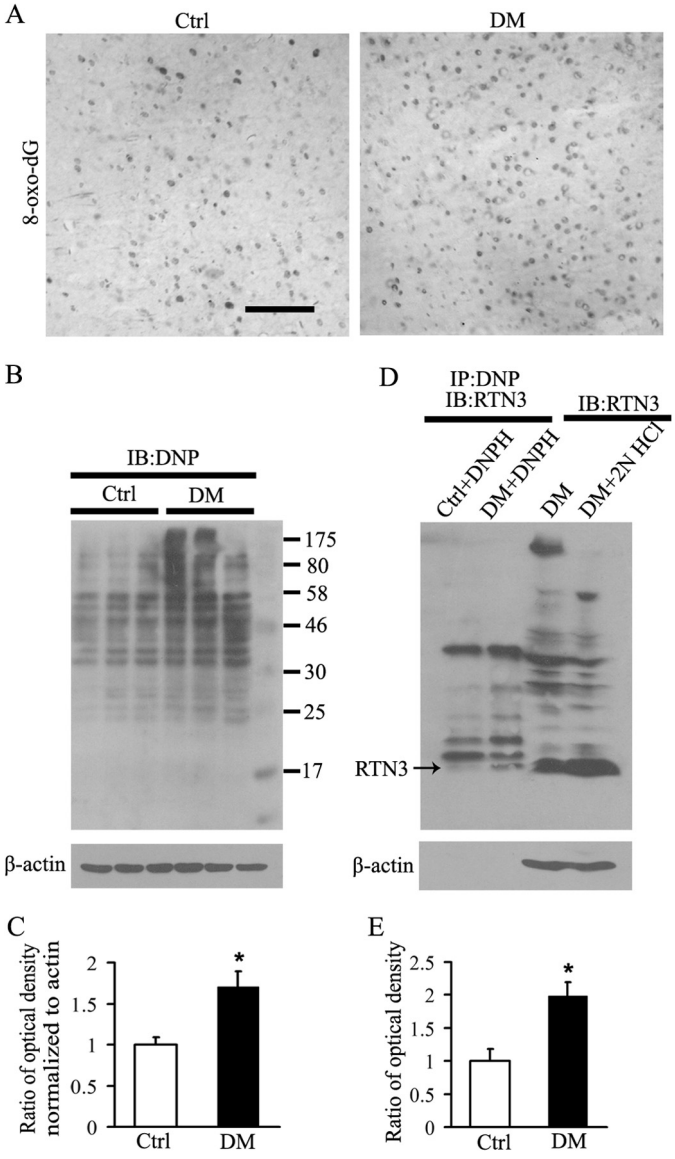

FIGURE 7. **Diabetes induced an increase in oxidative DNA and protein damage in rat brain.** *A*, immunostaining for 8-oxo-dG, a marker of oxidative DNA damage, revealed positive cell staining (8-oxo-dG$^+$) in both control (*Ctrl*) and diabetic (*DM*) brains. *Bar* = 100 μm. *B* and *C*, rat brain extracts were derivatized with 10 mM DNPH in 2 N HCl and detected with an antibody against DNP on Western blots to identify protein carbonyls. Western blotting (*IB*; *B*) shows a statistically significant increase in the number and density of protein carbonyls in DM brain (*C*). *D* and *E*, extracts from rat brains were immunoprecipitated (*IP*) with DNP antibody after DNPH derivatization and then probed with anti-RTN3 antibody to detect RTN3 carbonyls (*first* and *second lanes*). The results showed that the mono-RTN3 band could be detected in diabetic brain tissues after immunoprecipitation with DNP antibody, indicating that diabetes induced the formation of RTN3 carbonyls in brain. RTN3 carbonyls were significantly increased in diabetic brains compared with controls. Treatment of extracts from diabetic brains with vehicle or 2 N HCl revealed that HW-RTN3 bands could be detected in the control sample (*third lane*) but not in the acid-treated sample (*fourth lane*), suggesting that HW-RTN3 aggregates were unstable in acidic conditions and dissociated to mono-RTN3. All values are reported as the means ± S.E. (n = 6 per group). * represents $p < 0.05$ compared with the controls.

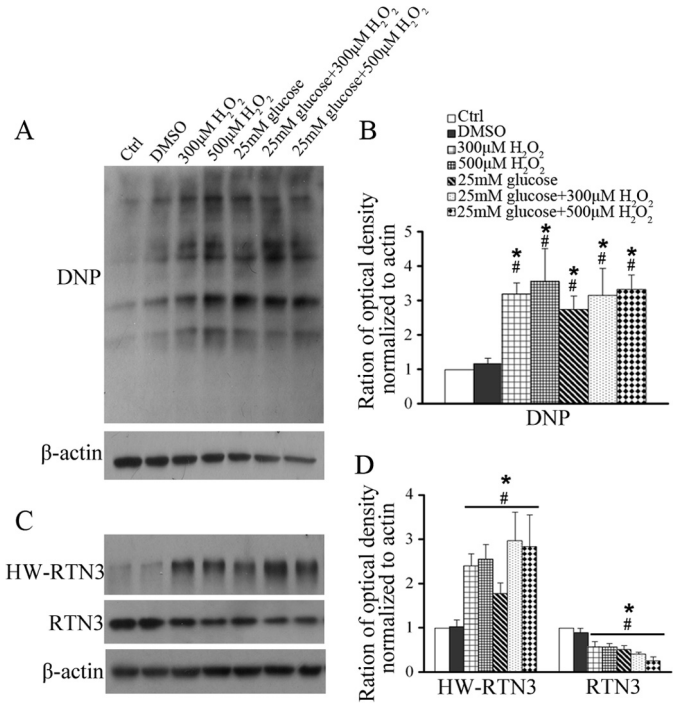

FIGURE 8. **High glucose induced the formation of protein carbonyls and RTN3 aggregates in SH-SY5Y cells.** Images representing the detection of protein carbonyls (*A*) and RTN3 (*C*) by Western blotting of the extracts from SH-SY5Y cells after 1 h of treatment with 300 μM H_2O_2, 500 μM H_2O_2, 25 mM glucose, 300 μM H_2O_2 + 25 mM glucose, 500 μM H_2O_2 + 25 mM glucose or 0.5% DMSO. Statistical data of *B* and *D* indicated that H_2O_2 and/or 25 mM glucose treatment induced significant increases in the amount of protein carbonyls (DNP) and HW-RTN3 and a decrease in monomeric RTN3 in SH-SY5Y cells. All values are reported as the means ± S.E. (n = 3–5 per group). * and # represent $p < 0.05$ *versus* the control and DMSO, respectively.

trophy in diabetic brains, similar to those defined as RIDNs. Evidence for this includes: 1) immunostaining for SMI32, an axonal marker, was significantly decreased in diabetic brains, indicating that axonal degeneration was apparent 2) RTN3 is normally distributed evenly in neuronal cell bodies and neurites, but in diabetic brains RTN3 became aggregated in neuritis, and 3) SMI32 protein was mainly expressed in neuronal cell bodies or in neurites without RTN3 aggregates. However, SMI32 staining was no longer observed in the neurites with RTN3 aggregates, showing the typical morphology of RIDNs (Fig. 6). These results demonstrated that neuritic dystrophy occurred in diabetic brains and was potentially mediated by endogenous oligomeric RTN3. Taken together, the reduction of RTN3 monomer and increase in RTN3 oligomer may synergistically induce neurotoxicity and neuritic dystrophy in diabetic brains.

Next, we studied the mechanisms underlying the changes in RTN3 expression in diabetic brains. The reduction of RTN3 monomer did not appear to be caused by abnormal transcription because RTN3 mRNA expression was similar in both diabetic and control rats (Fig. 3). Although the exact mechanism is unknown, our biochemical results demonstrate that a reduction of mono-RTN3 is associated with abnormal posttranslational processing. It has been reported that oxidative protein damage facilitates the formation of protein oligomers (38, 39), which can further inhibit protein degradation via the proteasome-mediated proteolytic pathway (40–42). In the present study, extensive oxidative damage of DNA and proteins in diabetic brains was observed by significantly increased 8-oxo-dG, a marker of oxidatively damaged DNA (43), and carbonylated proteins, major products of ROS-mediated oxidation reactions on proteins (42, 44, 45), respectively (Fig. 7*B*). Additionally,

severe oxidative damage of RTN3 was indicated by the presence of carbonylated RTN3 in diabetic brains (Fig. 7*D*). We treated the SH-SY5Y neuronal cell line with high glucose and/or H_2O_2 treatment to mimic high glucose and oxidative stress (46–48). Interestingly, we found that such stress conditions mimicked the effects observed in diabetic brains, *i.e.* increased formation of protein carbonyls and HW-RTN3, as well as a reduction of mono-RTN3 (Fig. 8). Both the *in vivo* and *in vitro* studies demonstrated for the first time that diabetes causes the formation of RTN3 aggregates via oxidative damage in the brain.

The normal morphology of neuronal dendrites and axons is fundamentally important to the development of neural plasticity, which is critical for maintaining cognitive functions (49). Here, we observed cognitive deficits in diabetic rats (Fig. 2). Although the exact mechanism underlying diabetes-induced cognitive deficits is still unclear, our findings suggest that RTN3 aggregates form in diabetic brain and cause neuritic dystrophy as indicated by RIDNs, which interrupts axonal and synaptic transmission. Moreover, Aβ processing was increased in diabetic brains via reduction of mono-RTN3 inhibitory effects on the activity of BACE1 enzyme. Soluble Aβ toxicity induces neuronal death via very complex mechanisms (50), including oxidative stress (51, 52). As mentioned above, oxidative stress induced RTN3 oxidative damage, which stimulated the formation of RTN3 aggregates and neuritic dystrophy and subsequently cognitive deficits. Therefore, diabetes-induced RTN3 oxidative damage may cause a vicious cycle that potentially accelerates neurodegeneration and cognitive dysfunction.

In the present study we also noticed that the increase of HW-RTN3- and RIDN-positive neurons could be readily detected in the cerebral cortex, but was significantly less in the hippocampus in this animal model (data not shown). This phenomenon might be related to the stages of neuropathogenesis in the brains after suffering diabetic dementia. PET scanning showed that Aβ deposits are mainly detected around the medial temporal and parietal cortical regions at the early stage of AD patients and spread globally to the other brain regions, including entire cortical and subcortical regions as well as brain stem, in the final stage of the disease (53). Moreover, functional magnetic resonance image data also demonstrate that task deactivation reduction and atrophy occur in the parietal cortical regions of the patients with mild cognitive impairment (54). Therefore, it is likely that progression of RIDNs formation in the different brain regions occurs at different stages of diabetic dementia. Future studies in this area might help us to find targets to prevent diabetic patients from onset of dementia.

In conclusion, the present study revealed that diabetes induces neuritic dystrophy in the brain of rats with cognitive deficits via protein oxidative damage. RTN3 formed aggregates/oligomers due to oxidative damage, which reduced its inhibitory effect on BACE1 activity and caused Aβ-mediated toxicity that led to neuronal death or neuritic dystrophy. The present findings provide the first evidence for the occurrence of RTN3 immunoreactive neuritic dystrophy in diabetic brains. Our molecular mechanistic study suggests that preventing oxidative damage will protect against neuritic dystrophy and reduce the risk of dementia for diabetic patients.

Acknowledgment—We sincerely thank Ya-Lin Huang for excellent technique assistance.

REFERENCES

1. Barnes, D. E., and Yaffe, K. (2011) The projected effect of risk factor reduction on Alzheimer's disease prevalence. *Lancet Neurol* **10,** 819–828
2. Grundke-Iqbal, I., Iqbal, K., Tung, Y. C., Quinlan, M., Wisniewski, H. M., and Binder, L. I. (1986) Abnormal phosphorylation of the microtubule-associated protein tau (tau) in Alzheimer cytoskeletal pathology. *Proc. Natl. Acad. Sci. U.S.A.* **83,** 4913–4917
3. Murrell, J., Farlow, M., Ghetti, B., and Benson, M. D. (1991) A mutation in the amyloid precursor protein associated with hereditary Alzheimer's disease. *Science* **254,** 97–99
4. Selkoe, D. J. (1986) Altered structural proteins in plaques and tangles. What do they tell us about the biology of Alzheimer's disease? *Neurobiol. Aging* **7,** 425–432
5. Spillantini, M. G., Goedert, M., Jakes, R., and Klug, A. (1990) Topographical relationship between β-amyloid and tau protein epitopes in tangle-bearing cells in Alzheimer disease. *Proc. Natl. Acad. Sci. U.S.A.* **87,** 3952–3956
6. Yankner, B. A. (1996) New clues to Alzheimer's disease. Unraveling the roles of amyloid and tau. *Nat. Med.* **2,** 850–852
7. O'Brien, J. T., and Burns, A. (2011) Clinical practice with anti-dementia drugs. A revised (second) consensus statement from the British Association for Psychopharmacology. *J. Psychopharmacol.* **25,** 997–1019
8. Daviglus, M. L., Bell, C. C., Berrettini, W., Bowen, P. E., Connolly, E. S., Jr., Cox, N. J., Dunbar-Jacob, J. M., Granieri, E. C., Hunt, G., McGarry, K., Patel, D., Potosky, A. L., Sanders-Bush, E., Silberberg, D., and Trevisan, M. (2010) National Institutes of Health State-of-the-Science Conference statement. Preventing alzheimer disease and cognitive decline. *Ann. Intern. Med.* **153,** 176–181
9. Shaw, J. E., Sicree, R. A., and Zimmet, P. Z. (2010) Global estimates of the prevalence of diabetes for 2010 and 2030. *Diabetes Res. Clin. Pract.* **87,** 4–14
10. Xu, W. L., von Strauss, E., Qiu, C. X., Winblad, B., and Fratiglioni, L. (2009) Uncontrolled diabetes increases the risk of Alzheimer's disease. A population-based cohort study. *Diabetologia* **52,** 1031–1039
11. Schrijvers, E. M., Witteman, J. C., Sijbrands, E. J., Hofman, A., Koudstaal, P. J., and Breteler, M. M. (2010) Insulin metabolism and the risk of Alzheimer disease. The Rotterdam Study. *Neurology* **75,** 1982–1987
12. Janson, J., Laedtke, T., Parisi, J. E., O'Brien, P., Petersen, R. C., and Butler, P. C. (2004) Increased risk of type 2 diabetes in Alzheimer disease. *Diabetes* **53,** 474–481
13. Murray, I. V., Proza, J. F., Sohrabji, F., and Lawler, J. M. (2011) Vascular and metabolic dysfunction in Alzheimer's disease. A review. *Exp. Biol. Med.* (*Maywood*) **236,** 772–782
14. Li, Z. G., Zhang, W., and Sima, A. A. (2007) Alzheimer-like changes in rat models of spontaneous diabetes. *Diabetes* **56,** 1817–1824
15. Zhang, T., Pan, B. S., Zhao, B., Zhang, L. M., Huang, Y. L., and Sun, F. Y. (2009) Exacerbation of poststroke dementia by type 2 diabetes is associated with synergistic increases of β-secretase activation and β-amyloid generation in rat brains. *Neuroscience* **161,** 1045–1056
16. Zhang, T., Pan, B. S., Sun, G. C., Sun, X., and Sun, F. Y. (2010) Diabetes synergistically exacerbates poststroke dementia and tau abnormality in brain. *Neurochem. Int.* **56,** 955–961
17. Xiong, M., Zhang, T., Zhang, L. M., Lu, S. D., Huang, Y. L., and Sun, F. Y. (2008) Caspase inhibition attenuates accumulation of β-amyloid by reducing β-secretase production and activity in rat brains after stroke. *Neurobiol. Dis.* **32,** 433–441
18. Tesco, G., Koh, Y. H., Kang, E. L., Cameron, A. N., Das, S., Sena-Esteves, M., Hiltunen, M., Yang, S. H., Zhong, Z., Shen, Y., Simpkins, J. W., and Tanzi, R. E. (2007) Depletion of GGA3 stabilizes BACE and enhances β-secretase activity. *Neuron* **54,** 721–737

19. Zhang, Y., Xiong, M., Yan, R. Q., and Sun, F. Y. (2010) Mutant ubiquitin-mediated β-secretase stability via activation of caspase-3 is related to β-amyloid accumulation in ischemic striatum in rats. *J. Cereb. Blood Flow Metab.* **30,** 566–575
20. Oertle, T., and Schwab, M. E. (2003) Nogo and its paRTNers. *Trends Cell Biol.* **13,** 187–194
21. Iwahashi, J., Kawasaki, I., Kohara, Y., Gengyo-Ando, K., Mitani, S., Ohshima, Y., Hamada, N., Hara, K., Kashiwagi, T., and Toyoda, T. (2002) *Caenorhabditis elegans* reticulon interacts with RME-1 during embryogenesis. *Biochem. Biophys. Res. Commun.* **293,** 698–704
22. Steiner, P., Kulangara, K., Sarria, J. C., Glauser, L., Regazzi, R., and Hirling, H. (2004) Reticulon 1-C/neuroendocrine-specific protein-C interacts with SNARE proteins. *J. Neurochem.* **89,** 569–580
23. Karnezis, T., Mandemakers, W., McQualter, J. L., Zheng, B., Ho, P. P., Jordan, K. A., Murray, B. M., Barres, B., Tessier-Lavigne, M., and Bernard, C. C. (2004) The neurite outgrowth inhibitor Nogo A is involved in autoimmune-mediated demyelination. *Nat. Neurosci.* **7,** 736–744
24. Yang, Y. S., and Strittmatter, S. M. (2007) The reticulons. A family of proteins with diverse functions. *Genome Biol.* **8,** 234
25. Parodi, J., Sepúlveda, F. J., Roa, J., Opazo, C., Inestrosa, N. C., and Aguayo, L. G. (2010) β-Amyloid causes depletion of synaptic vesicles leading to neurotransmission failure. *J. Biol. Chem.* **285,** 2506–2514
26. Yan, R., Shi, Q., Hu, X., and Zhou, X. (2006) Reticulon proteins. Emerging players in neurodegenerative diseases. *Cell. Mol. Life Sci.* **63,** 877–889
27. Tang, B. L., and Liou, Y. C. (2007) Novel modulators of amyloid-β precursor protein processing. *J. Neurochem.* **100,** 314–323
28. Murayama, K. S., Kametani, F., Saito, S., Kume, H., Akiyama, H., and Araki, W. (2006) Reticulons RTN3 and RTN4-B/C interact with BACE1 and inhibit its ability to produce amyloid β-protein. *Eur. J. Neurosci.* **24,** 1237–1244
29. Hu, X., Shi, Q., Zhou, X., He, W., Yi, H., Yin, X., Gearing, M., Levey, A., and Yan, R. (2007) Transgenic mice overexpressing reticulon 3 develop neuritic abnormalities. *EMBO J.* **26,** 2755–2767
30. Shi, Q., Prior, M., He, W., Tang, X., Hu, X., and Yan, R. (2009) Reduced amyloid deposition in mice overexpressing RTN3 is adversely affected by preformed dystrophic neurites. *J. Neurosci.* **29,** 9163–9173
31. Nelson, P. T., Smith, C. D., Abner, E. A., Schmitt, F. A., Scheff, S. W., Davis, G. J., Keller, J. N., Jicha, G. A., Davis, D., Wang-Xia, W., Hartman, A., Katz, D. G., and Markesbery, W. R. (2009) Human cerebral neuropathology of type 2 diabetes mellitus. *Biochim. Biophys. Acta* **1792,** 454–469
32. Zhang, F., Ye, C., Li, G., Ding, W., Zhou, W., Zhu, H., Chen, G., Luo, T., Guang, M., Liu, Y., Zhang, D., Zheng, S., Yang, J., Gu, Y., Xie, X., and Luo, M. (2003) The rat model of type 2 diabetic mellitus and its glycometabolism characters. *Exp. Anim.* **52,** 401–407
33. Morris, R. (1984) Developments of a water-maze procedure for studying spatial learning in the rat. *J. Neurosci. Methods* **11,** 47–60
34. Liu, H. M., Yang, S. Z., and Sun, F. Y. (2010) 1-Methyl-4-phenyl-pyridinium time-dependently alters expressions of oxoguanine glycosylase 1 and xeroderma pigmentosum group F protein in PC12 cells. *Neurosci. Bull.* **26,** 1–7
35. Lortz, S., Tiedge, M., Nachtwey, T., Karlsen, A. E., Nerup, J., and Lenzen, S. (2000) Protection of insulin-producing RINm5F cells against cytokine-mediated toxicity through overexpression of antioxidant enzymes. *Diabetes* **49,** 1123–1130
36. He, W., Lu, Y., Qahwash, I., Hu, X. Y., Chang, A., and Yan, R. (2004) Reticulon family members modulate BACE1 activity and amyloid-β peptide generation. *Nat. Med.* **10,** 959–965
37. Prior, M., Shi, Q., Hu, X., He, W., Levey, A., and Yan, R. (2010) RTN/Nogo in forming Alzheimer's neuritic plaques. *Neurosci. Biobehav. Rev.* **34,** 1201–1206
38. Squier, T. C. (2001) Oxidative stress and protein aggregation during biological aging. *Exp. Gerontol.* **36,** 1539–1550
39. Hashimoto, M., Rockenstein, E., Crews, L., and Masliah, E. (2003) Role of protein aggregation in mitochondrial dysfunction and neurodegeneration in Alzheimer's and Parkinson's diseases. *Neuromolecular Med.* **4,** 21–36
40. Powell, S. R., Wang, P., Divald, A., Teichberg, S., Haridas, V., McCloskey, T. W., Davies, K. J., and Katzeff, H. (2005) Aggregates of oxidized proteins (lipofuscin) induce apoptosis through proteasome inhibition and dysregulation of proapoptotic proteins. *Free Radic. Biol. Med.* **38,** 1093–1101
41. Lee, M. H., Hyun, D. H., Jenner, P., and Halliwell, B. (2001) Effect of proteasome inhibition on cellular oxidative damage, antioxidant defenses, and nitric oxide production. *J. Neurochem.* **78,** 32–41
42. Dalle-Donne, I., Aldini, G., Carini, M., Colombo, R., Rossi, R., and Milzani, A. (2006) Protein carbonylation, cellular dysfunction, and disease progression. *J. Cell. Mol. Med.* **10,** 389–406
43. Cheng, K. C., Cahill, D. S., Kasai, H., Nishimura, S., and Loeb, L. A. (1992) 8-Hydroxyguanine, an abundant form of oxidative DNA damage, causes G-T and A-C substitutions. *J. Biol. Chem.* **267,** 166–172
44. Dalle-Donne, I., Rossi, R., Colombo, R., Giustarini, D., and Milzani, A. (2006) Biomarkers of oxidative damage in human disease. *Clin. Chem.* **52,** 601–623
45. Dalle-Donne, I., Giustarini, D., Colombo, R., Rossi, R., and Milzani, A. (2003) Protein carbonylation in human diseases. *Trends Mol. Med.* **9,** 169–176
46. Wang, W., Sun, F., An, Y., Ai, H., Zhang, L., Huang, W., and Li, L. (2009) Morroniside protects human neuroblastoma SH-SY5Y cells against hydrogen peroxide-induced cytotoxicity. *Eur. J. Pharmacol.* **613,** 19–23
47. Vincent, A. M., Brownlee, M., and Russell, J. W. (2002) Oxidative stress and programmed cell death in diabetic neuropathy. *Ann. N.Y. Acad. Sci.* **959,** 368–383
48. Greene, D. A., Stevens, M. J., Obrosova, I., and Feldman, E. L. (1999) Glucose-induced oxidative stress and programmed cell death in diabetic neuropathy. *Eur. J. Pharmacol.* **375,** 217–223
49. Selkoe, D. J. (2002) Alzheimer's disease is a synaptic failure. *Science* **298,** 789–791
50. Glabe, C. G., and Kayed, R. (2006) Common structure and toxic function of amyloid oligomers implies a common mechanism of pathogenesis. *Neurology* **66,** S74–S78
51. Sponne, I., Fifre, A., Drouet, B., Klein, C., Koziel, V., Pinçon-Raymond, M., Olivier, J. L., Chambaz, J., and Pillot, T. (2003) Apoptotic neuronal cell death induced by the non-fibrillar amyloid-β peptide proceeds through an early reactive oxygen species-dependent cytoskeleton perturbation. *J. Biol. Chem.* **278,** 3437–3445
52. De Felice, F. G., Velasco, P. T., Lambert, M. P., Viola, K., Fernandez, S. J., Ferreira, S. T., and Klein, W. L. (2007) Aβ oligomers induce neuronal oxidative stress through an *N*-methyl-D-aspartate receptor-dependent mechanism that is blocked by the Alzheimer drug memantine. *J. Biol. Chem.* **282,** 11590–11601
53. Ewers, M., Sperling, R. A., Klunk, W. E., Weiner, M. W., and Hampel, H. (2011) Neuroimaging markers for the prediction and early diagnosis of Alzheimer's disease dementia. *Trends Neurosci.* **34,** 430–442
54. Threlkeld, Z. D., Jicha, G. A., Smith, C. D., and Gold, B. T. (2011) Task deactivation reductions and atrophy within parietal default mode regions are overlapping but only weakly correlated in mild cognitive impairment. *J. Alzheimers Dis.* **27,** 415–427